The Journal of Chemical Physics

RESEARCH ARTICLE | JULY 28 2023

Elimination of the bias-stress effect in ligand-free quantum dot field-effect transistors

Jason Tolentino; Markelle Gibbs ; Alex Abelson ; Matt Law

J. Chem. Phys. 159, 044709 (2023)
https://doi.org/10.1063/5.0152100

The Journal of Chemical Physics ARTICLE pubs.aip.org/aip/jcp

Elimination of the bias-stress effect in ligand-free quantum dot field-effect transistors

Cite as: J. Chem. Phys. 159, 044709 (2023); doi: 10.1063/5.0152100
Submitted: 27 March 2023 • Accepted: 10 July 2023 •
Published Online: 28 July 2023

Jason Tolentino,[1] Markelle Gibbs,[2] Alex Abelson,[3] and Matt Law[1,2,3,a)]

AFFILIATIONS

[1]Department of Chemical Engineering and Materials Science, University of California, Irvine, Irvine, California 92697, USA
[2]Department of Chemistry, University of California, Irvine, Irvine, California 92697, USA
[3]Department of Materials Science and Engineering, University of California, Irvine, Irvine, California 92697, USA

Note: This paper is part of the JCP Special Topic on 40 Years of Colloidal Nanocrystals in JCP.
[a)]**Author to whom correspondence should be addressed:** matt.law@uci.edu

ABSTRACT

Field-effect transistors (FETs) made from colloidal quantum dot (QD) solids commonly suffer from current–voltage hysteresis caused by the bias-stress effect (BSE), which complicates fundamental studies of charge transport in QD solids and the use of QD FETs in electronics. Here, we show that the BSE can be eliminated in *n*-channel PbSe QD FETs by first removing the QD ligands with a dose of H_2S gas and then infilling the QD films with alumina by atomic layer deposition (ALD). The H_2S-treated, alumina-infilled FETs have stable, hysteresis-free device characteristics (total short-term stability), indefinite air stability (total long-term stability), and a high electron mobility of up to 14 $cm^2\ V^{-1}\ s^{-1}$, making them attractive for QD circuitry and optoelectronic devices. The BSE-free devices are utilized to conclusively establish the dependence of the electron mobility on temperature and QD diameter. We demonstrate that the BSE in these devices is caused by both electron trapping at the QD surface and proton drift within the film. The H_2S/alumina chemistry produces ligand-free PbSe/PbS/Al_2O_3 interfaces that lack the traps that cause the electronic part of the BSE, while full alumina infilling stops the proton motion responsible for the ionic part of the BSE. Our matrix engineering approach should aid efforts to eliminate the BSE, boost carrier mobilities, and improve charge transport in other types of nanocrystal solids.

INTRODUCTION

Colloidal quantum dot (QD) thin-film field-effect transistors (FETs) are important devices for studying charge transport in QD solids and fabricating QD-based electronics.[1,2] Unfortunately, QD FETs commonly exhibit hysteresis in their current–voltage characteristics caused by the bias-stress effect (BSE). The BSE occurs when the application of a gate bias (V_G) triggers the accumulation of immobile charges near the gate/channel interface that progressively screens the gate field and causes a time-dependent (transient) decay of the mobile carrier density and drain current (I_D) in the channel. The immobile charges can be electrons/holes that are trapped in pre-existing or bias-induced traps or ions such as protons, hydroxide ions, and charged ligands that are pre-existing or induced by the bias stress. In addition to causing I_D decay, progressive screening of the gate field also increases the magnitude of the gate voltage needed to induce a conducting channel (the threshold voltage, V_T). V_T shifts and I_D transients under an applied gate bias are hallmarks of the BSE (Fig. 1). Figures 1(b) and 1(c) show generic electronic and ionic processes that can cause the BSE in QD FETs.

The BSE has been a persistent problem for PbX (X = S, Se, and Te) QD FETs.[1–17] In our own work,[4–6,8,10,17] we have viewed the BSE as a curiosity, an annoyance, and a reason to better understand charge transport in these systems. Hysteresis and an unstable I_D complicate measurements of transport physics and device performance (e.g., carrier mobility) and prevent the use of these transistors in applications that require stable device characteristics. In cases where the BSE transients are sufficiently slow, a workaround for charge transport studies is to scan current–voltage (I–V) curves as fast as possible to minimize the hysteretic distortions caused by the transients,[8] but this tactic sometimes fails.[17] It would be better to find a way to eliminate the BSE altogether. Proposed causes of the BSE in PbX QD FETs include dynamic charge trapping by either the ligands,[9] QD surface defects such as Pb dimers,[18] or

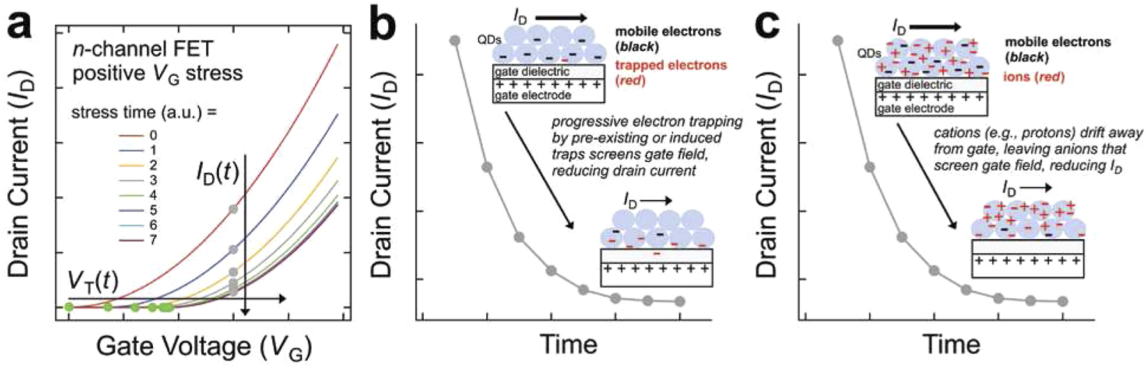

FIG. 1. The bias-stress effect in QD FETs. (a) Schematic time evolution of the transfer (I_D–V_G) plot of an *n*-channel FET suffering from the BSE. Upon application of a constant positive gate bias (the bias stress), a progressive build-up of immobile charges near the gate/channel interface screens the gate field, increasing V_T (green dots) and decreasing I_D with time for a fixed set of biasing conditions (e.g., gray dots). The transfer curves are idealized by the authors as a set of shifted and scaled parabolas. (b)–(c) Depictions of generic electronic and ionic mechanisms of the BSE. $I_D(t)$ shows a quasi-exponential decay upon application of a positive gate bias as (b) trapped electrons or (c) drifting ions (e.g., protons) screen the gate field.

H_2O/O_2 adsorbates within the QD films.[13] However, these hypotheses are unproven, and there has been very limited progress in making BSE-free devices. The standard remedy of employing hydroxyl-free gate dielectrics with low interfacial trap densities[19,20] is usually ineffective for PbX QD FETs, which indicates that the immobile charges responsible for the BSE tend to accumulate within the QD films, not on the surface or in the bulk of the gate dielectric.[4,9,13,21] Zhou *et al.* tried to stop the BSE in *p*-channel PbS QD FETs by inserting a MoO_{3-x} electron blocking layer at the source/drain electrodes, but large transients remained after the electrode modification.[15] Our group achieved strong suppression (but not complete elimination) of BSE transients in Na_2S-treated PbSe QD FETs by infilling the QD films with amorphous aluminum oxide (alumina) using atomic layer deposition (ALD).[10] Now we describe an improved matrix engineering approach that utilizes H_2S-induced ligand removal and alumina infilling to completely eliminate the BSE in PbSe QD FETs, yielding hysteresis-free *n*-channel transistors with high electron mobilities. We show that the BSE is caused by both charge trapping at the QD surface and proton motion within the films and demonstrate that BSE elimination requires both the formation of a ligand-free PbSe/PbS/alumina interface (which removes the traps responsible for the electronic part of the BSE) and full infilling of the QD film with an ALD coating (which stops the proton motion that causes the ionic part of the BSE). The introduction of BSE-free PbX QD FETs should accelerate progress in charge transport studies and optoelectronic applications of QD solids.

RESULTS AND DISCUSSION

Figure 2(a) shows the three-step process that we used to fabricate PbSe QD FETs that are free of the bias-stress effect (see Methods). We began by depositing conductive amorphous QD films onto prepatterned FET substrates [p^{++} (100)-oriented Si coated with a 200 nm thick SiO_2 layer and patterned with metal source and drain electrodes (5 nm Cr/45 nm Au)] using layer-by-layer dip coating[4,8] to quantitatively replace the native oleate ligands with small ligands that have a high vapor pressure when in their neutral protonated form, such as 1,2-ethanedithiolate (EDT^{2-}), formate ($HCOO^-$), or thiocyanate (SCN^-). Next, the samples were exposed to a dose of H_2S gas in a glovebox-integrated ALD chamber to protonate the small ligands, which then quantitatively evaporated from the QD films as neutral molecules, leaving behind films that are presumably capped with about one monolayer of HS^- ligands. Finally, in the third step, the QD films were infilled and overcoated with amorphous alumina (a-Al_2O_3)[10,22] in the same ALD chamber to produce all-inorganic, ligand-free, *n*-channel QD FETs that show zero BSE transients at room temperature. As we explain below, the key to eliminating the BSE in these devices is to (i) fully remove the ligands to produce atomically clean PbSe/PbS/Al_2O_3 interfaces with a relatively low concentration of electron traps, and (ii) fully infill the QD films to prevent internal ion (proton) motion. We found that the H_2S-treated, alumina-infilled QD FETs showed very similar performance characteristics—including high linear electron mobility (3–14 $cm^2\ V^{-1}\ s^{-1}$), total long-term air stability,[10,22] and zero BSE transients (no current-voltage hysteresis)—regardless of which small volatile ligand was used in their fabrication.

We evaluated the performance of these bottom-contact, global back gate FETs [Fig. 2(b)] at room temperature. Figures 2(c)–2(l) show representative results for EDT-capped devices (6.3 nm diameter QDs). Prior to any ALD treatments (H_2S or a-Al_2O_3), the EDT-capped devices behaved as ambipolar transistors with relatively low electron and hole mobility and significant drain current (I_D) hysteresis due to prominent BSE transients [Figs. 2(c) and 2(d)].[4] Exposing the FETs to one pulse of H_2S at a substrate temperature of 54 °C caused a dramatic change in their current–voltage characteristics: the FETs became *p*-channel transistors featuring quasi-linear output plots, weak gate modulation of I_D, and somewhat slower I_D transients [Figs. 2(e) and 2(f)]. These H_2S-dosed devices behaved in a very similar fashion to sulfide-capped FETs

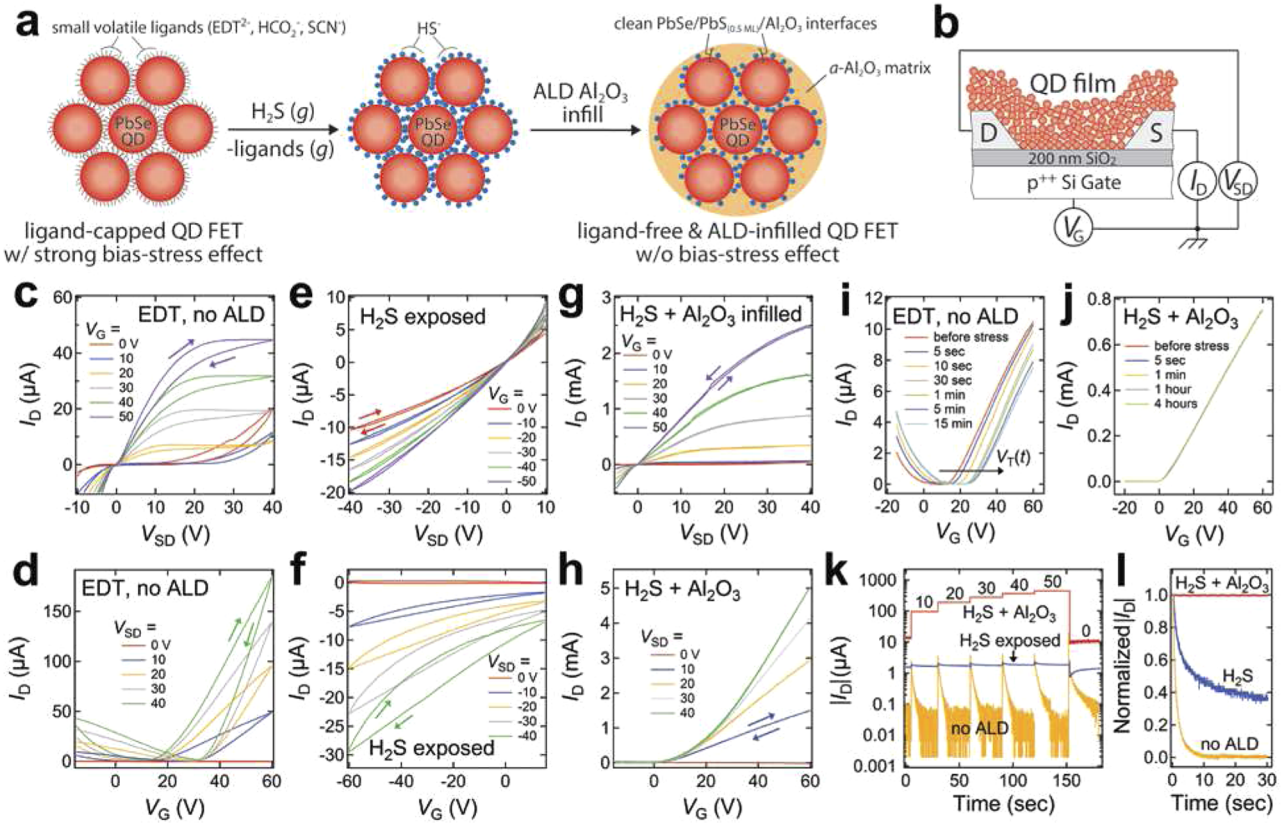

FIG. 2. Design of BSE-free QD FETs and examples using EDT-treated PbSe QD films. (a) The fabrication process. A dose of H_2S gas protonates and completely removes a volatile ligand such as EDT, formate, or thiocyanate from the surface of a PbSe QD film. Subsequent deposition of alumina by low-temperature ALD produces a ligand-free, atomically clean PbSe/PbS/Al_2O_3 interface and an ALD-infilled QD FET with negligible bias-stress transients at room temperature. (b) The FET geometry. (c) Room-temperature output (I_D–V_{SD}) and (d) transfer (I_D–V_G) plots for a typical EDT-capped FET, and the corresponding plots (e)–(f) after exposure to a single pulse of H_2S gas in the ALD chamber followed by (g)–(h) infilling and overcoating with a-Al_2O_3 by ALD, all at a substrate temperature of 54 °C. Arrows denote sweep directions. Sweep rates = 50 V/s. The linear electron mobility of the H_2S-treated, alumina-infilled FET determined at V_{SD} = 10 V and V_G = 50 V is 3.9 $cm^2\ V^{-1}\ s^{-1}$. (i) Transfer plots (at V_{SD} = 5 V) for an EDT-capped device (no ALD) after various durations of bias stress (V_G = 40 V and V_{SD} = 5 V), showing significant V_T shifts due to the BSE. (j) Similar transfer plots for an H_2S-capped, alumina-infilled FET showing zero BSE after even four hours of continuously applied bias (also at V_G = 40 V and V_{SD} = 5 V). (k) Log-linear plots of $|I_D|$ vs time for these devices at $|V_{SD}|$ = 5 V. Labels denote $|V_G|$. (l) Normalized plots of $|I_D|$ vs time after stepping $|V_G|$ from 20 to 30 V ($|V_{SD}|$ = 5 V). The current of the H_2S-dosed, alumina-infilled device is completely stable (no I_D transient). QD diameter = 6.3 nm; QD film thickness = 30–40 nm; alumina thickness = 20 nm. Channel dimensions: length = 25 μm and width = 1000 μm. T = 298 K. See Fig. S1 in the supplementary material for additional data on devices made from EDT-capped QDs.

previously prepared in our laboratory by solution-phase ligand exchange with Na_2S.[10] The similarity in behavior is likely due to the abundance of electronically active sulfides (S^{2-} or SH^-) adsorbed on the surface of the QDs in both types of films.[11] Remarkably, upon fully infilling and overcoating the H_2S-dosed devices with amorphous alumina using ALD at 54 °C, the FETs became n-channel transistors with high linear electron mobility (3–4 $cm^2\ V^{-1}\ s^{-1}$), insignificant hysteresis in output plots, and negligible BSE transients at room temperature [Figs. 2(g) and 2(h)]. Transfer plots acquired as a function of bias stress soaking time clearly show the absence of BSE in the H_2S-treated, alumina-infilled FETs [Figs. 2(i) and 2(j)]. We also characterized I_D vs time by measuring I_D at a constant source–drain voltage (V_{SD}) while stepping the gate voltage (V_G) from 0 to ±50 V in 10 V increments. Figures 2(k) and 2(l) are log-linear and normalized plots of $|I_D|$ vs time for these devices. While both the EDT-capped and H_2S-dosed devices exhibited quasi-exponential I_D transients after each step in V_G, the H_2S-dosed and alumina-infilled device showed no transients. A linear plot of these data confirmed that the absence of the transients is real, not an artifact of y-axis scaling and higher device conductivity (Fig. S1 in the supplementary material). The staircase-like shape of the I_D vs time plots is characteristic of a well-behaved FET that responds to sudden changes in V_G with sudden and stable changes in I_D. This H_2S/alumina surface chemistry produces what is to our knowledge the first example of a PbX QD FET without hysteresis at room temperature.

We found that the BSE transients were eliminated by the combination of H_2S dosing and alumina infilling only when volatile ligands were used to produce the initial QD films. For example, both formic acid (HCOOH) and hydrocyanic acid (HSCN) have

high vapor pressures[23,24] and, thus, readily evaporate at the substrate temperatures used for H_2S dosing (54–75 °C). Fourier transform infrared (FTIR) spectra show that exposing formate- or thiocyanate-capped QD films to an H_2S pulse of 3×10^6 Langmuir (L) at 54 °C results in the complete loss of all ligand vibrational signatures (Fig. 3). The carboxylate peaks of adsorbed formate at 1554 and 1327 cm^{-1} and the characteristic –C≡N stretch of thiocyanate at 2021 cm^{-1} disappeared after H_2S exposure (blue traces). This is consistent with protonation and evaporation of the ligands by H_2S. Subsequent infilling with ALD alumina caused little additional change to the FTIR spectra, but the resulting FETs were free of transients (red traces in Fig. 3) and showed I–V plots that were nearly identical to those of H_2S-treated and alumina-infilled FETs made from EDT-capped QD films (Figs. S2 and S3). The electron mobility of these FETs is independent of the V_G sweep rate used to acquire the transfer plots from which the mobility values are extracted (Fig. S4). As with the EDT-capped films, both H_2S ligand exchange *and* alumina infilling were required to eliminate the transients of formate- and thiocyanate-capped films. H_2S exposure alone removed the ligands but worsened the transients (blue traces), while infilling alone removed most of the ligands but only part of the transients (gray traces). Optical absorption spectra indicated that a similar amount of redshifting and broadening of the first exciton absorption peak occurred for the EDT-, formate-, and thiocyanate-capped films upon H_2S dosing and again upon infilling (Figs. S1–S3). The excitonic peak remained distinct and narrow for all films, indicating that the H_2S and infilling steps did not cause a significant increase in the polydispersity of the QDs by etching, necking, sintering, or ripening.

As a check on the above-mentioned results, we verified that the BSE transients persisted if nonvolatile ligands were used to prepare the initial QD films. Figure 4 shows FTIR and I_D time trace data for films capped with oxalate, trimesate, and 1,4-benzenedithiolate (BDT) ligands, each of which has a very low vapor pressure as a neutral molecule.[25] As expected, H_2S dosing did not remove these ligands from the films because the ligands do not appreciably evaporate when protonated. Indeed, the absence of C=O and S–H peaks in the FTIR spectra of H_2S-dosed films suggests that these three ligands are not protonated by H_2S to any significant extent. Since the neutral ligands are kinetically trapped on the QD surface in the absence of solvent, any ephemerally protonated ligands are likely to quickly back react to expel H_2S. Subsequent alumina infilling also had little impact on the ligand loading of the films. All the FETs made using nonvolatile ligands showed strong BSE transients, with the magnitude and time constants of the transients varying somewhat for the different ligands and steps in the fabrication process (Fig. 4 and Figs. S5–S7). Our data show that ligand removal is a necessary but insufficient condition for eliminating the transients. Complete elimination of the transients requires ligand removal with H_2S and infilling/overcoating of the QDs with alumina. As discussed in more detail below, the strong correlation between the chemical state of the QD surface and the presence of transients suggests that the electron BSE in our *n*-channel PbSe QD FETs is caused by screening of the applied gate field by species on the surface of the QDs rather than on or in the gate dielectric or near the source/drain contacts. It is likely that QDs with "dirty," ligand-covered, or poorly passivated surfaces suffer particularly strong BSE transients.

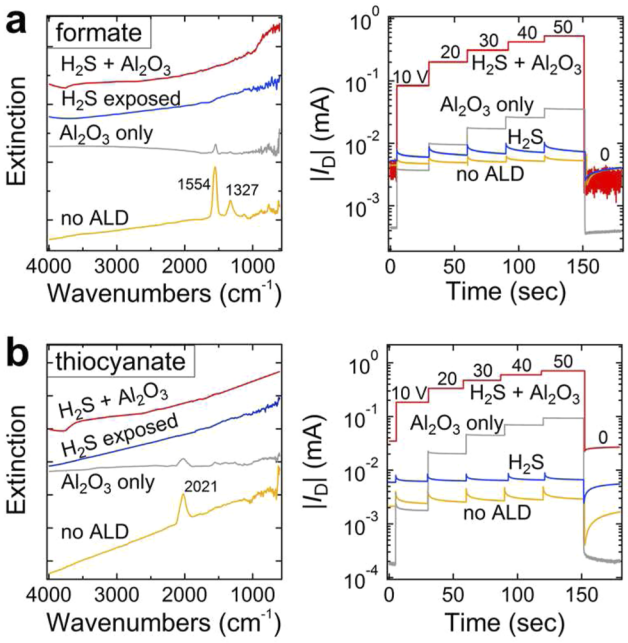

FIG. 3. Volatile ligands produce PbSe QD FETs free of the BSE. FTIR spectra and log-linear $|I_D|$ time traces for films made from (a) formate-capped and (b) thiocyanate-capped PbSe QD films. The spectra show complete loss of the ligands upon exposure to H_2S (orange vs blue traces). Subsequent alumina deposition results in insignificant additional changes to the spectra (red traces). The H_2S-treated, alumina-infilled FETs show negligible BSE, but infilled devices made without H_2S exposure have both residual ligand and noticeable I_D transients (gray traces). Labels on the time traces denote $|V_G|$. $|V_{SD}| = 5$ V. The linear electron mobility of the H_2S-treated and alumina-infilled FETs made from the formate- and thiocyanate-capped films is 3.4 and 4.7 $cm^2\ V^{-1}\ s^{-1}$, respectively. All processing conditions and FET parameters are the same as in Fig. 2. See Figs. S2 and S3 for additional data on films made using these two volatile ligands.

The stable device characteristics of the BSE-free FETs enabled the first unambiguous determination of the dependence of electron mobility on temperature and QD size. Figure 5(a) shows the dependence of the linear electron mobility on temperature (80–300 K) for H_2S-treated and alumina-infilled FETs made from SCN- or EDT-capped films of 6.1 nm diameter QDs. The mobility is weakly thermally activated ($d\mu/dT > 0$) for both types of FETs and increased by only 35%–40% over this temperature range. The simple Arrhenius nearest-neighbor hopping expression $\mu(T) = \mu_\infty \exp(-E_A/kT)$ with a temperature-independent prefactor μ_∞ yielded reasonable fits of the data using very small E_A values of 3–4 meV (data not shown). These activation energies are similar to values recently reported for hole transport in single-grain PbSe QD superlattice transistors[17] and suggest that carriers follow low-barrier percolative pathways through the films.[8] Whereas the superlattice FETs suffered from thermally-activated BSE transients that suppressed the high-temperature mobility, created (in whole or part) a negative $d\mu/dT$ region above ~150 K, and rendered $\mu(T)$ ambiguous, the BSE-free amorphous FETs studied here show unambiguous $\mu(T)$ curves that are consistent with hopping transport.

Figure 5(b) shows the room-temperature electron mobility of FETs made from EDT-capped films as a function of QD diameter. In 2010, we reported that the electron mobility of EDT-capped PbSe QD FETs has a maximum at a QD diameter of ~6 nm (lower orange trace).[8] However, the devices used in that study suffered from fast and diameter-dependent BSE transients. Despite employing even faster V_G sweeps to acquire transfer curves, we could not be certain at the time that our measured mobility values and resulting mobility-size plots were unaffected by the transients. Here, we reproduced our previous work and found that devices without H_2S dosing and alumina infilling showed the same size dependence as before, but with slightly higher mobility values (upper orange trace). After H_2S treatment and alumina infilling, the BSE transients were eliminated and the mobility values increased by about an order of magnitude, but the basic size dependence of the mobility was unchanged (red trace). These data confirm that our previously-reported dependence of the electron mobility on QD size is real, not an artifact of the BSE. These results also demonstrate that the H_2S/alumina chemistry eliminates the BSE for a range of QD diameters.

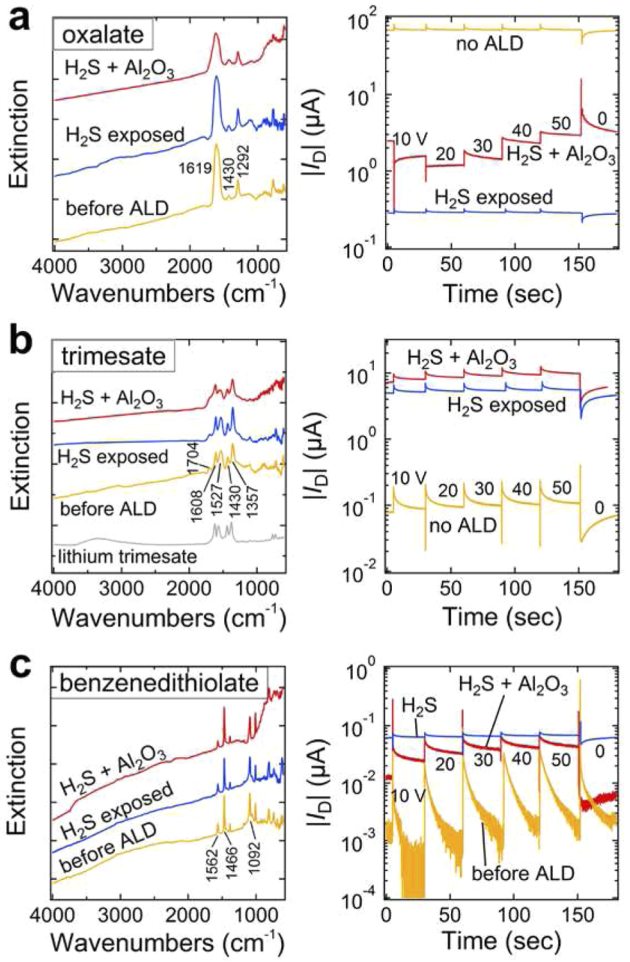

FIG. 4. Non-volatile ligands yield PbSe QD FETs that retain significant BSE transients. FTIR spectra and log-linear $|I_D|$ time traces for films made from (a) oxalate-, (b) trimesate-, and (c) 1,4-benzenedithiolate-capped QDs. The spectra show that the non-volatile ligands on the as-made films (orange traces) are not removed by H_2S exposure (blue traces) or subsequent alumina infilling (red traces). All devices, including the H_2S-treated and alumina-infilled FETs, show significant I_D transients. Labels on the time traces denote $|V_G|$. $|V_{SD}|$ = 5 V. All processing conditions and FET parameters are the same as in Fig. 2. See Figs. S5–S7 for additional data on films made using these three non-volatile ligands.

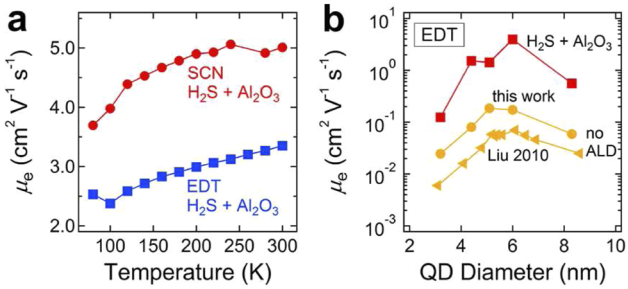

FIG. 5. Mobility trends for BSE-free QD FETs. (a) Linear electron mobility as a function of temperature for FETs made from thiocyanate-capped (red) and EDT-capped (blue) QD films. See Fig. S8 for transfer curves and I_D time traces for these devices. (b) Room-temperature electron mobility as a function of QD diameter for FETs made from EDT-capped films. Data are shown for devices without H_2S treatment and alumina infilling (orange traces) and with H_2S treatment and alumina infilling (red trace). See Fig. S9 for current–voltage and time trace data for the BSE-free FETs made from 3.2, 4.4, 5.1, and 8.3 nm QDs. All FET and ALD parameters are the same as in Fig. 2.

Increasing the ALD temperature from 54 to 75 °C substantially increased the FET mobilities. As with the devices made at 54 °C, the highest mobilities were achieved using thiocyanate-capped QD films (Figs. 2, 3, and 5). Figure 6 shows representative data for thiocyanate-capped films dosed with H_2S and infilled with alumina at 75 °C, which we know from past work is a sufficiently low temperature to avoid QD sintering and coarsening during ALD.[19] We measured a room-temperature electron mobility of 12–14 $cm^2\ V^{-1}\ s^{-1}$ for these FETs [Fig. 6(b)]. These are the highest-mobility PbX QD FETs made by our group to date. The devices combine high electron mobility with negligible BSE/hysteresis (i.e., total short-term stability) and indefinite air stability (i.e., total long-term stability).[10,22] We speculate that the higher ALD temperature improves the electron mobility by producing a higher-quality PbSe/PbS/alumina interface and alumina coating that better passivate the QD surface.

To determine how the H_2S/alumina chemistry eliminates the BSE in our ligand-free QD FETs, we began by verifying that the transients are associated with the surface of the QDs rather than the gate dielectric or FET contacts. We tested many different treatments and modifications of the bare FET substrates, including annealing up to 200 °C in different environments, plasma treatments, self-assembled monolayers, the use of alumina as a gate dielectric, the use of different source/drain contact metals, and various combinations of H_2S dosing and alumina coating prior to depositing the QD films (Fig. S11), but these efforts failed to significantly suppress the BSE transients. The fact that the transients were eliminated only by H_2S/alumina treatment of the QD films further convinced us that the BSE in these *n*-FETs is caused by the accumulation of immobile charge within the QD films rather than in other parts of these devices.

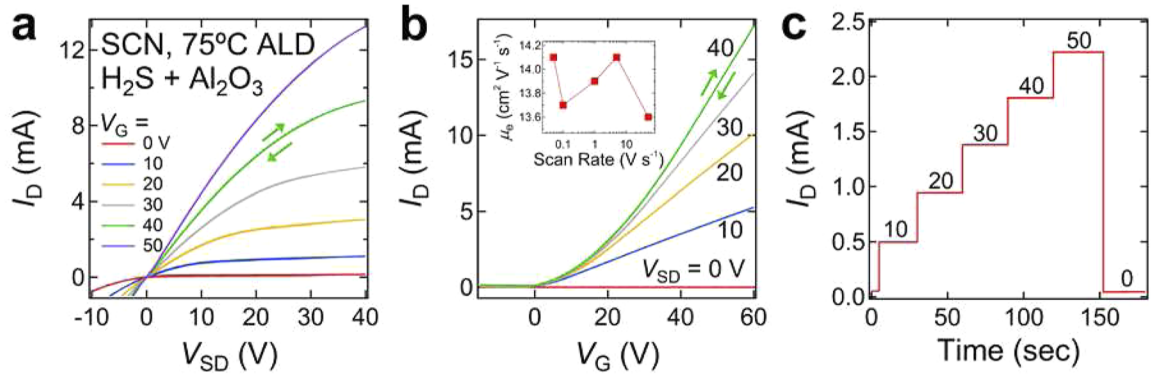

FIG. 6. High-mobility BSE-free PbSe QD FETs. Typical room-temperature (a) output and (b) transfer curves for FETs made from thiocyanate-capped QD films dosed with H_2S and infilled with alumina at 75 °C. The electron mobility of this device is 12.5 $cm^2\ V^{-1}\ s^{-1}$. Inset is a plot of the mobility vs V_G sweep rate for a similar device, showing an effectively constant mobility of ~13.9 ± 0.2 $cm^2\ V^{-1}\ s^{-1}$. (c) Representative I_D time traces for these devices. Labels denote V_G. V_{SD} = 5 V. Other device and measurement parameters are the same as in Fig. 2. See Fig. S10 for additional data on these films and devices.

We next measured the elemental composition of the H_2S-treated and alumina-infilled films by secondary ion mass spectrometry (SIMS) depth profiling to gain insight into the nature of the QD/alumina interfaces produced by the H_2S dosing and alumina infilling processes. To set a baseline for SIMS studies of the films, we first determined the amount of sulfur and other elemental impurities in a bulk powder of our oleate-capped PbSe QDs using glow discharge mass spectrometry (GDMS). GDMS provides a full elemental survey (Li–U) with ppb–ppm detection limits.[26] The GDMS data, compiled in Table I, showed a total of 15 elements above the limit of detection out of 74 elements quantified. Note that matrix elements (Pb and Se), gas-forming elements (H, C, N, O, and noble gases), and radioactive elements were not quantified in this analysis. The elements above 1 ppm (equivalent to ~5×10^{16} atoms cm^{-3} in the QD film, see Methods) were phosphorus (2040 ppm), silicon (31 ppm), chlorine (25 ppm), sulfur (6 ppm), boron (3.1 ppm), calcium (1.3 ppm), aluminum (1.0 ppm), sodium (1.0 ppm), and bismuth (0.94 ppm). For the purposes of this paper, the most important conclusion from the GDMS data is that the sulfur content of our as-made QDs was quite low (<10 ppm), which is a prerequisite for studying the sulfur content of the H_2S treated and infilled films (see below). However, several other aspects of the GDMS data are noteworthy. First, the high level of phosphorus (equivalent to ~15% of a monolayer on the QD surfaces) is reasonable given the use of trioctylphosphine selenide (TOP-Se) and diphenylphosphine (DPP) in the QD synthesis. We speculate that the phosphorus is present mostly as adsorbed molecular species derived from DPP and TOP-Se rather than as point defects in the PbSe lattice. Second, ignoring phosphorus, a total impurity content of only ~70 ppm is striking because, on the one hand, the QDs were surprisingly pure despite a lack of special effort on our part to ensure high-purity conditions, but, on the other hand, several of the impurities were in sufficiently high concentration to act as dopants, traps, and recombination centers in the QD films (particularly Si, Cl, B, Al, and Na). A better understanding of the location and electronic behavior of these impurities is needed to determine whether they may cause deep traps that limit the performance of QD optoelectronic devices.

TABLE I. GDMS elemental analysis of as-made oleate-capped PbSe QD powder. Unlisted elements were below detection limits. See Fig. S12 for the GDMS analysis report and the method used to convert the data from ppm wt. to ppm at.

Element	ppm wt.	ppm at.	Atoms/cm^3
P	3000	2040	1×10^{20}
Si	41	31	1.5×10^{18}
Cl	40	25	1.2×10^{18}
Bi	9.2	0.94	4.6×10^{16}
S	9	6	3×10^{17}
Ca	2.4	1.3	6.2×10^{16}
B	1.6	3.1	1.5×10^{17}
Al	1.3	1.0	5.0×10^{16}
Na	1.1	1.0	5.0×10^{16}
Zn	0.57	0.18	9.0×10^{15}
Ni	0.28	0.10	4.9×10^{15}
Fe	0.15	0.057	2.8×10^{15}
V	0.1	0.04	2×10^{15}
Ti	0.07	0.03	2×10^{15}
Mn	0.02	0.008	4×10^{14}

We used SIMS mainly to quantify the amount of sulfur present at the $PbSe/Al_2O_3$ interface of our BSE-free FETs. Initially, we hypothesized that the SH^- adsorbed on the QDs during H_2S treatment would be removed by H_2O during subsequent *a*-Al_2O_3 ALD, resulting in clean $PbSe/Al_2O_3$ interfaces. However, SIMS showed that about 0.4 monolayers (MLs) of sulfur (1.5×10^{21} atoms cm^{-3}) remained on the surface of the QDs when formate-capped films were dosed with H_2S and then infilled with alumina in the standard way. This sulfur content is the same as that of Na_2S-treated, ALD-infilled PbSe QD films previously reported by our group.[10] SIMS control experiments on a formate-capped film infilled with alumina without intentional exposure to H_2S (or any other source of sulfur)

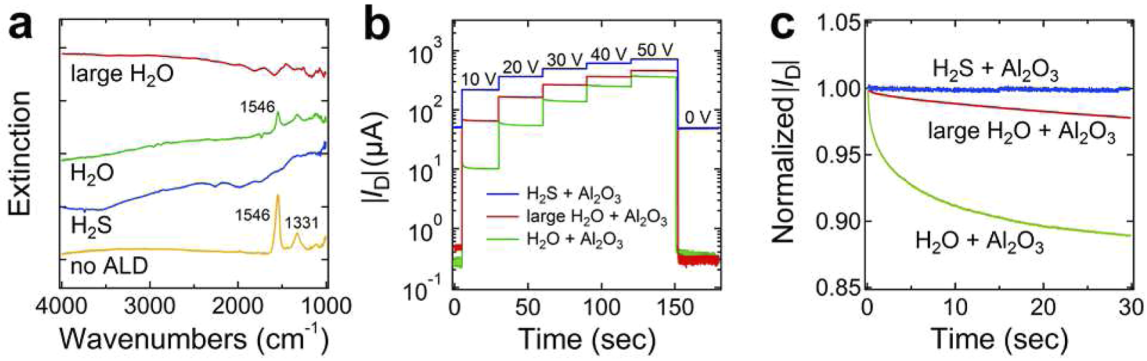

FIG. 7. Large doses of H_2O can remove volatile ligands, yielding nearly transient-free FETs after alumina infilling without H_2S. (a) Typical FTIR spectra of formate-capped QD films before ALD (orange), after a 3×10^6 L dose of H_2S (blue) or H_2O (green), and after a 3×10^7 L dose of H_2O (red) at 54 °C. H_2S treatment resulted in complete ligand exchange, while the same dose of H_2O removed only a fraction of the formate. The larger dose of H_2O was required to exchange all of the formate. (b) $|I_D|$ time traces of the corresponding alumina-infilled FETs. The transients were absent in the H_2S-dosed device, very weak in the device made by complete ligand exchange with a large H_2O dose, and substantial in the device made by incomplete ligand exchange with a normal dose of H_2O. Labels on the time traces denote V_G. V_{SD} = 5 V. (c) Normalized plots of $|I_D|$ vs time after stepping V_G from 20 to 30 V (V_{SD} = 5 V). The transient was suppressed but not eliminated by using a large dose of H_2O prior to alumina infilling. All device and measurement parameters are the same as in Fig. 2. See Fig. S14 for *I–V* data of infilled FETs made using complete ligand exchange with H_2O.

showed a sulfur concentration about 19 times lower (8×10^{19} atoms cm^{-3} = 1740 ppm, or about 2% of a monolayer; Fig. S13), confirming that the sulfur observed in the transient-free films came from H_2S exposure rather than some uncontrolled background source. We cannot, at present, account for why the sulfur concentration of the supposedly sulfur-free infilled films was so much higher than that of the as-made QD powder measured by GDMS (1740 ppm vs 6 ppm), but adventitious adsorption of thiols from the atmosphere of our glovebox (e.g., EDT) during the fabrication of the films may be responsible. Additional control experiments on a benzenedithiolate-capped film infilled with alumina without any exposure to H_2S showed tenfold higher sulfur and carbon levels and fourfold higher hydrogen levels than the transient-free film, consistent with the retention of BDT ligands after ALD, as seen in IR spectra (Fig. S13 and Fig. 4). All three films had similar amounts of phosphorus ($6–10 \times 10^{18}$ at. cm^{-3}). The SIMS results show that the structure of the QD/alumina interface in the BSE-free FETs is $PbSe/PbS_{(\sim 0.4\ ML)}/Al_2O_3$ rather than $PbSe/Al_2O_3$.

We have demonstrated that *in vacuo* dosing with H_2S quantitatively protonates and desorbs volatile anionic ligands from the surface of the QD films. H_2O dosing was found to work in a similar fashion, but larger doses of H_2O were needed to achieve complete ligand exchange because H_2O is a significantly weaker acid than H_2S.[27] The IR spectra in Fig. 7(a) show the degree of ligand removal for formate-capped QD films exposed to different doses of H_2S and H_2O gas. As seen from the spectra, an H_2S dose of 3×10^6 Langmuir (L) was sufficient to remove all formate from the film surface. In our ALD system, this dose was obtained by

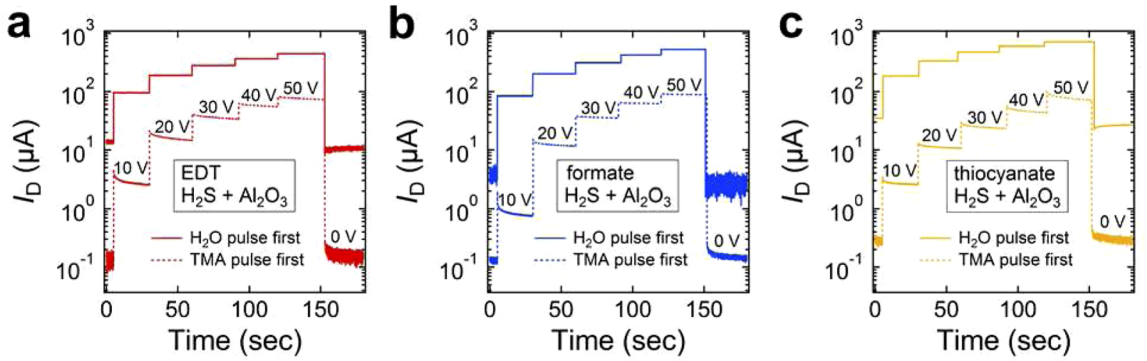

FIG. 8. Initiating ALD alumina deposition with H_2O eliminates the transients, but starting with TMA does not. I_D time traces for H_2S-treated, alumina-infilled FETs made from (a) EDT-, (b) formate-, and (c) thiocyanate-capped QDs. Solid traces correspond to devices in which the alumina deposition was initiated with a pulse of H_2O (our normal procedure). Note that the transients are eliminated and the currents are relatively large. Dashed traces correspond to devices in which the alumina deposition was initiated with a pulse of TMA. Note that the transients are sizable and the currents are smaller. Labels on the time traces denote V_G. V_{SD} = 5 V. All device and measurement parameters are the same as in Fig. 2. See Fig. S15 for these data plotted on a linear scale.

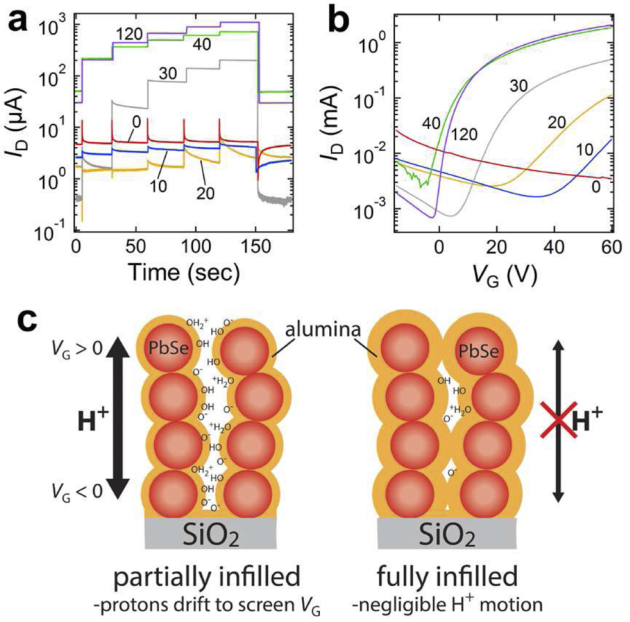

FIG. 9. Full ALD infilling is required to eliminate the BSE transients. (a) Typical log-linear I_D time traces (V_{SD} = 5 V) and (b) transfer curves (V_{SD} = 10 V) as a function of the number of cycles of ALD alumina. Sample details: 6.2 nm, EDT-capped PbSe QDs exposed to H_2S and infilled at 54 °C. All other device and measurement parameters are the same as in Fig. 2(c) Cartoon depicting the proposed proton drift mechanism of the BSE. (*left*) Mobile protons on the continuous internal alumina surface of partially-infilled films can move to screen the applied gate field, causing some or all of the observed BSE. (*right*) "Fully" infilled films have a small number of mostly small, isolated pores, so the protons that exist within these films cannot move to screen the gate field. This is why films must be completely infilled to eliminate the BSE transients. See Fig. S17 for additional *I–V* data for these samples and Fig. S18 for the data for FETs made from thiocyanate-capped QDs using an ALD temperature of 75 °C.

either a single large pulse (P_{max} ~ 1 Torr) or seven smaller pulses (P_{max} ~ 0.12 Torr) of H_2S. The same dose of H_2O removed only 60%–70% of the formate, but we could achieve quantitative removal of formate with a tenfold larger dose of H_2O (~3×10^7 L). If the formate was removed by H_2S, subsequent infilling with alumina eliminated the BSE transients (Fig. 3). If a large dose of H_2O was used instead, the transients of the infilled, ligand-free films were suppressed but not eliminated [Figs. 7(b) and 7(c)]. It therefore seems that some amount of sulfur at the PbSe/Al_2O_3 interface is beneficial for the complete elimination of the transients. The sulfur sub-monolayer may also be responsible for the higher conductivity of H_2S-treated films [Fig. 7(b)]. The much larger I_D of the H_2S-dosed devices at V_G = 0 V [Fig. 7(b)] was due to a more negative threshold voltage V_T for the H_2S-treated FETs (V_T = −6 V, compared to V_T ~ 0 V for H_2O-treated FETs) and is not indicative of a lower on/off ratio.

Let us review what is known about the BSE transients so far. They are (i) thermally activated;[7,9,10,17] (ii) associated with the surface of the QDs rather than the gate dielectric or contacts; (iii) eliminated by ligand exchange with H_2S followed by coating the QDs with ALD alumina to form PbSe/$PbS_{(\sim 0.4\ ML)}$/Al_2O_3 interfaces; (iv) suppressed but not eliminated by ligand exchange with large doses of H_2O followed by alumina coating. Since the transients are very sensitive to the chemistry of the QD surface, we next tested how they responded to changing (1) the pulse sequence used for alumina deposition, (2) the thickness of the alumina coating, and (3) the ALD material used to infill the QD FETs after H_2S exchange.

We found that the transients were eliminated only if alumina deposition was initiated with a pulse of H_2O. Starting instead with a pulse of trimethylaluminum (TMA) after H_2S dosing resulted in FETs with sizable BSE transients and lower conductivity, regardless of which ligand (EDT, formate, or thiocyanate) was used to make the QD films (Fig. 8). This suggests that the transients are caused by electronic states or mobile species on the PbSe surface that are better passivated by starting the alumina ALD sequence with H_2O instead of TMA. Starting with H_2O may passivate surface Pb ions that are not already coordinated with SH^-, thereby eliminating surface states while also providing a more hydroxylated QD surface for better alumina nucleation and growth. In contrast, starting with TMA likely creates Pb–S–$Al(Me)_2$ species on the surface that sterically block the coordination of unpassivated Pb ions by H_2O and lead to a patchier and lower-quality alumina coating as a result.

Not only is the ALD pulse sequence important for eliminating the transients, but so also is the thickness of the alumina coating. We measured a series of FETs made by infilling H_2S-treated QD films with different thicknesses of alumina (0, 10, 20, 30, 40, and 120 ALD cycles) deposited by beginning with an H_2O pulse. Figure 9(a) shows that the transients became gradually weaker with an increasing number of ALD cycles and completely disappeared for devices made with at least 40 cycles (about the number needed to fully infill these QD films[10]). The *I–V* characteristics of these devices also showed a continuous evolution with the number of ALD cycles: the threshold voltage shifted from >60 V (at 0 cycles) to −4 ± 2 V (at ≥40 cycles), an *n*-channel appeared and gradually dominated the FET behavior, and the electron mobility increased from 0.71 to 1.9, 4.9, and 5.4 $cm^2\ V^{-1}\ s^{-1}$ for 20, 30, 40, and 120 ALD cycles, respectively [Fig. 9(b)]. A similar progression was observed during alumina infilling of Na_2S-treated QD FETs.[10] TEM imaging showed that the alumina formed a continuous conformal coating at all thicknesses, with no evidence for island formation (Fig. S16). Thus, the fact that the transients stopped only after the QD films were fully infilled with alumina (at ~40 cycles) rather than once the PbSe/PbS surface was passivated by the first few ALD cycles suggests that the BSE was at least partly caused by the drift of ions along the internal free surfaces of the films. We reasoned that protons on the QD and alumina surfaces could migrate in the transverse direction along the internal surface of the interconnected pore network of unfilled and partially-infilled films in response to V_G. In this picture, when V_G > 0 V, protons are gradually repelled from the channel, leaving a sheet of immobile $-O^-$ (oxide) anions that progressively screens V_G and causes the BSE [Figs. 9(c) and 1(c)]. Fully infilling the films should fill much of the pore space and isolate the residual pores from each other, thereby preventing surface protons from drifting to screen V_G [Fig. 9(c)]. We note that Song *et al.* recently attributed *I–V* hysteresis in PbS QD solar cells and FETs to mobile protons within the QD films.[28]

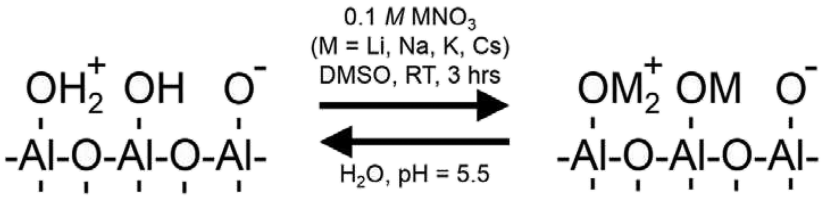

SCHEME 1. Alkali cation exchange on the internal alumina surface of partially-infilled QD films. The alumina surface is naturally hydroxylated, terminated by –OH, $–O^-$, and $–OH_2^+$ groups. Partially infilled FETs were soaked in 0.1 M solutions of alkali nitrates in anhydrous DMSO to replace surface protons with alkali cations ($M^+ = Li^+$, Na^+, K^+, or Cs^+). The cation exchange was reversible by soaking the devices in degassed water.

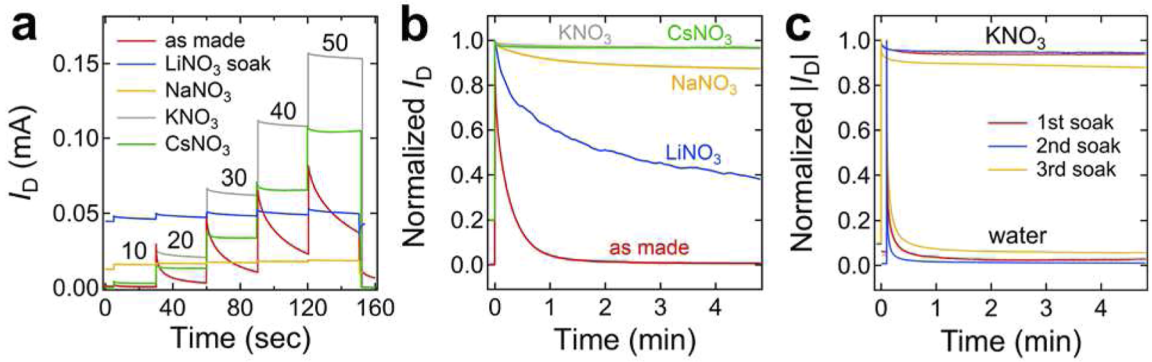

FIG. 10. Replacing surface protons with larger monovalent cations suppresses the BSE of partially-infilled QD FETs. (a) Typical I_D time traces for partially-infilled FETs (6.2 nm QDs, thiocyanate-capped, H_2S-dosed, 25 cycles of alumina at 54 °C) soaked in different 0.1 M MNO_3 solutions for three hours. Labels indicate V_G values. V_{SD} = 5 V. (b) Normalized I_D time traces for such devices as a function of MNO_3 treatment upon stepping V_G from 0 to 40 V (V_{SD} = 5 V). The transient is progressively weakened after treatment with larger alkali cations. (c) Overlaid normalized $|I_D|$ time traces for a device that was soaked in KNO_3/DMSO and then water three times, showing that the transient suppression is reversible. $|V_{SD}|$ = 5 V and $|V_G|$ was stepped from 0 to 40 V. All other device and measurement parameters are the same as in Fig. 2. See Fig. S19 for additional data on the devices presented here and Fig. S20 for results on control devices soaked in pure DMSO.

To test the hypothesis that proton drift is a cause of the BSE, we carried out alkali metal cation exchange studies of partially-infilled QD FETs. Thiocyanate-capped FETs dosed with H_2S and partially infilled with alumina (25 cycles at 54 °C) were soaked for three hours in 0.1 M solutions of alkali metal nitrates (MNO_3) in anhydrous dimethyl sulfoxide (DMSO) at room temperature to replace surface protons with Li^+, Na^+, K^+, or Cs^+ ions (Scheme 1). We reasoned that these larger, heavier ions should be less mobile than protons, and the transients of the cation-exchange devices would weaken if proton drift was indeed a significant cause of the BSE. Figure 10(a) shows that the transients were dramatically suppressed after the MNO_3 soaks. $LiNO_3$ soaks suppressed the transients the least, while KNO_3 and $CsNO_3$ soaks suppressed them the most [Fig. 10(b)]. Stronger transient suppression by the larger cations can be explained by their smaller surface diffusivities and/or more complete exchange of surface protons. We found that the transient suppression was reversible by soaking the devices in pure water to reprotonate their surfaces [Fig. 10(c)]. Control experiments confirmed that the transients were affected predominantly by the alkali metal cations, not the DMSO or anion (Figs. S20–S22). From these studies, we conclude that proton drift is a second cause of the BSE in our FETs and that full infilling stops proton drift and eliminates the associated BSE transients by closing off pathways for proton motion.

We also investigated whether the BSE transients could be eliminated by ALD infills other than alumina. Full ZnO, ZnS, CdO, and TiO_2 infills were tested on H_2S-dosed devices processed at 54 °C. Infilling with ZnO produced *n*-channel FETs with very weak transients, while ZnS and CdO infilling gave *n*-FETs with strong transients and TiO_2 infilling yielded *p*-FETs with strong transients (Fig. S23). The failure of these four alternative infills to eliminate the transients shows that there is something special about the H_2S/alumina chemistry. Indeed, we found that ZnO and TiO_2 infills eliminated the transients if they were deposited on at least one cycle of ALD alumina. For example, while weak transients remained in thiocyanate-capped FETs dosed with H_2S and infilled with 250 cycles of ZnO, the transients were absent in FETs infilled with 1–10 cycles of Al_2O_3 followed by 250 cycles of ZnO (Fig. S24). Similarly, we made BSE-free *n*-FETs from EDT-capped films infilled with 20 cycles of alumina followed by 20 cycles of ZnO or TiO_2 (Fig. S25). These experiments show that the critical requirements for eliminating the transients are to produce a clean PbSe/PbS/alumina interface

and then fully infill the films by ALD. The formation of the ligand-free PbSe/PbS/alumina interface evidently reduces charge trapping on the QD surfaces (the electronic mechanism of the BSE), while full infilling stops proton drift within the films (the ionic mechanism of the BSE).

Finally, we note that while H_2S dosing and alumina infilling eliminated the electron transients, residual hole transients persisted after the H_2S/alumina treatment. Close inspection of transfer curves reveals that the *n*-FETs had very weak *p*-channels at negative V_G [e.g., Fig. 2(h) and Figs. 2S3(h), and S26]. I_D time traces in the hole conduction regime at negative V_G showed significant BSE transients, despite the elimination of such transients in the electron conduction regime at positive V_G (Fig. S26). We did not study the hole transients in detail, so we can only speculate that they are caused by hole traps on the surface of the QDs or SiO_2 gate dielectric that are not passivated by the H_2S/alumina chemistry. Additional or alternative treatments may be required to eliminate hole transients and hole-related *I*–*V* hysteresis in PbSe QD FETs.

CONCLUSION

Transistors made from colloidal QD solids frequently suffer hysteresis from the BSE, which can complicate fundamental studies of charge transport and limit the development of practical QD-based electronics. We showed here that the BSE can be eliminated in PbSe QD *n*-FETs by H_2S ligand exchange and alumina infilling with ALD. The resulting H_2S-dosed, alumina-infilled FETs have stable, hysteresis-free device characteristics (total short-term stability), indefinite air stability (total long-term stability), and a high electron mobility up to 14 $cm^2\ V^{-1}\ s^{-1}$, making them attractive *n*-FETs for constructing high-performance QD circuits and optoelectronic devices. These BSE-free devices were used to unambiguously demonstrate how the electron mobility depends on temperature and QD diameter, illustrating the importance and utility of hysteresis-free devices in basic research. The high mobility of the BSE-free FETs is likely a product of reduced charge trapping, enhanced electronic coupling, and the absence of I_D transients (the latter of which cause systematic underestimation of the carrier mobility).

Our work has revealed evidence for both an electronic and ionic mechanism of the BSE in PbSe QD FETs. The H_2S/alumina chemistry produces ligand-free PbSe/$PbS_{(\sim 0.4\ ML)}$/Al_2O_3 interfaces that lack the charge traps that cause the electronic part of the BSE. Meanwhile, full alumina infilling stops proton drift along the internal surfaces of the QD films, which is responsible for the ionic part of the BSE. The formation of a clean PbSe/PbS/Al_2O_3 interface was found to be essential for eliminating the BSE transients. Modifications to our standard H_2S/alumina process, including the use of nonvolatile ligands, H_2O rather than H_2S dosing, TMA-first ALD pulse sequences, partial infilling, and infilling with ALD materials other than alumina, failed to eliminate the BSE, suggesting that recipes for BSE elimination may be quite specific and different for different types of QD solids. We nevertheless believe that (i) ligand removal and surface passivation to stop charge trapping and (ii) ALD infilling to stop ion motion are good initial design goals in ongoing efforts to eliminate the BSE in other QD transistors.[17]

MATERIALS AND METHODS

Chemicals. All chemicals were used as received unless otherwise noted. Lead oxide (PbO, 99.999%), selenium shot (99.999%), $LiNO_3$ (99%), and KNO_3 (99.0%) were purchased from Alfa Aesar. Oleic acid (OA, technical grade, 90%), diphenylphosphine (DPP, 98%), 1-octadecene (ODE, 90%), anhydrous hexanes (99%), anhydrous ethanol (≥99.5%), anhydrous methanol (99.8%), anhydrous acetonitrile (99.99%), anhydrous dimethyl sulfoxide (DMSO, ≥99.9%), anhydrous tetrachloroethylene (TCE, 99%), extra dry acetone (99.8%), acetone (>99.5%) and isopropanol (>99.5%) for substrate cleaning outside of the glovebox, 1,2-ethanedithiol (>98%), ammonium thiocyanate (99.99%), formic acid (98%), oxalic acid (≥99%), trimesic acid (95%), 1,4-benzenedithiol (BDT, 99%), 3-mercaptopropyltrimethoxysilane (3-MPTMS, 95%), sodium hydroxide (97%), $NaNO_3$ (≥99.0%), $CsNO_3$ (99.99%), $LiClO_4$ (≥98.0%), $NaClO_4$ (≥98.0%), tetrabutylammonium nitrate (97%), tetrabutylammonium perchlorate (≥99.0%), trimethylaluminum (97%), titanium tetrachloride (≥99.995%), and diethylzinc were purchased from Sigma-Aldrich. Trioctylphosphine (technical grade, >90%) was acquired from Fluka and mixed with Se shot for 24 h to form a 1 M trioctylphosphine-Se stock solution. Gold shot (99.99%), titanium, aluminum, and silver pieces, chromium plated tungsten rods, and molybdenum evaporation boats were purchased from Kurt Lesker. H_2S gas (99.3%) was purchased from Airgas. 18.2 MΩ water (Milli-Q Gradient) was used for substrate cleaning, atomic layer deposition (ALD), and cation exchange experiments. For ALD and other experiments inside the glovebox, the water was freeze-pump-thawed three times prior to use.

PbSe Quantum Dot Synthesis. PbSe QDs were synthesized and purified using standard air-free techniques. In a typical synthesis, 1 g of PbO, 5 g of oleic acid, and 15 g of ODE were mixed in a three-neck round-bottom flask and degassed at 80 °C under vacuum until a clear solution was formed. Once the solution became transparent, it was heated at 180 °C for at least 1 hour to dry the solution. While heating, 15 ml of 1 M TOP-Se solution containing 0.2 ml of DPP was rapidly injected into the hot solution. The QDs were grown for preselected times (30 s–5 min) depending on the desired QD size. The reaction was then quenched with a water bath and 15 ml of anhydrous hexane. The QDs were purified in an N_2-filled glovebox (<0.1 ppm O_2 and H_2O) by three rounds of redispersion and precipitation using hexanes and ethanol/methanol and stored as a powder in the glovebox.

QD film deposition. PbSe QD films were prepared by using a layer-by-layer procedure described elsewhere using a mechanical dip coater mounted inside a glovebox (DC Multi-8, Nima Technology). Briefly, substrates (microscope glass slide, silicon, quartz, or prepatterned FET substrates, all typically cleaned by sonication in Triton X-100 detergent and isopropanol followed by drying under N_2 flow) were alternately dipped into a 5 mg ml^{-1} solution of QDs in anhydrous hexanes and then a solution of the desired short-chain ligand: 1 mM EDT, BDT, formic acid, trimesic acid, or oxalic acid in anhydrous acetonitrile, or 0.5 mM NH_4SCN in anhydrous acetone. In the case of BDT, NH_4SCN, oxalic acid, and trimesic acid, a third beaker containing neat acetonitrile or acetone was used to rinse the films after each dip in the ligand treatment to remove any ligand residue. We fabricated films with thicknesses in a range of 30–200 nm (thin for FETs, thicker for XRD and optical absorption studies).

Atomic layer deposition. H_2S dosing was performed in a homemade cold-wall traveling wave ALD system within a glovebox at a substrate temperature of 54 or 75 °C. H_2S gas was introduced using computer-controlled diaphragm valves in-line with a 100 SCCM stream of N_2 carrier gas. H_2S doses up to 3×10^6 Langmuir (L) were obtained using either single long pulses ($P \sim 1$ Torr) or a series of shorter pulses ($P \sim 0.12$ Torr), with identical effects. H_2O dosing was performed in the same fashion but with exposures up to 3×10^7 L.

Amorphous alumina (a-Al_2O_3) was deposited in the same ALD system from trimethylaluminum and water at a substrate temperature of 54 or 75 °C and an operating pressure of ~0.1 Torr. Pulse and purge times were 20 ms and 120 s, respectively. The alumina growth rate was ~1.1 Å per cycle at these temperatures.

Polycrystalline ZnO, ZnS, and CdO infills were grown by ALD using diethylzinc and water, diethylzinc and H_2S, and dimethyl cadmium and water, respectively. Amorphous TiO_2 infills were grown by ALD using $TiCl_4$ and water. All precursors were used at room temperature, and the substrate temperature was 54 °C.

MNO_3 treatments. Metal nitrate treatments of partially-infilled QD FETs (~2.5 nm alumina) were performed in the glovebox. Samples were soaked in 0.1 M MNO_3 in anhydrous DMSO at room temperature for 3 h and then rinsed with anhydrous DMSO and blown dry. All other salt treatments (e.g., $LiClO_4$, $TBANO_3$) were performed in the same way. Soaks in degassed water (also in the glovebox) were used to reverse the cation exchange.

Characterization. Transmission electron microscopy (TEM) imaging was performed using a Philips CM20 operating at 200 kV. SEM images were acquired using an FEI Magellan 400 instrument operating at 10 kV and 100 pA. Optical extinction spectra of films on glass or quartz substrates were acquired using a PerkinElmer Lambda 950 spectrophotometer operating in the transmission mode. Films not protected from air with an ALD overcoat were sealed in optical cells consisting of two mated 1.33″ ConFlat sapphire viewports. FTIR transmission spectra of QD films on double-side polished intrinsic Si substrates were acquired in dry air using a Nicolet 6700 spectrometer at a resolution of 4 cm^{-1} with a blank Si substrate as the background. X-ray diffraction patterns of QD films were collected using a Rigaku SmartLab with Cu Kα irradiation.

Glow discharge mass spectrometry (GDMS) measurements of oleate-capped QD powders were performed by Evans Analytical Group using a VG 9000 GDMS instrument (Thermo Scientific). The powder was pressed into high-purity In foil (99.99999%) previously cleaned with acid to remove surface impurities. Impurities in the In foil were analyzed prior to the elemental analysis of each sample. Glow discharge conditions of 1.0 kV, 2.0 mA, and 100 Pa of 99.9999% Ar were used for all measurements. Samples were presputtered for 5 min prior to data acquisition. The intensities of the ion beams were measured using a Faraday cup for lead, selenium, and indium isotopes and a Daly conversion detector for all analytes in the samples. The efficiency of the detectors was calibrated using ^{180}Ta (relative isotopic abundance of 0.012%) measured using the Daly detector and ^{181}Ta (relative isotopic abundance of 99.99%) measured using the Faraday cup during analysis of pure Ta metal. Scan points per peak were 70 channels, DAC steps of 7, and integration times of 100 and 160 ms for the Daly detector and Faraday cup, respectively.

Secondary ion mass spectrometry (SIMS) of alumina-infilled films on silicon substrates was performed by Evans Analytical Group using a Physical Electronics ADEPT-1010 dynamic SIMS instrument using a 1 keV Cs ion beam for anions (S, O, H, C, P, Si, Al, and Se). Estimated lower detection limits for elements in the alumina overlayer were 1×10^{19} atoms cm^{-3} for sulfur and hydrogen, 1×10^{18} atoms cm^{-3} for carbon, and 1×10^{17} atoms cm^{-3} for phosphorus and silicon. The detection limits for elements in the silicon substrate were 1×10^{19} atoms cm^{-3} for hydrogen, 5×10^{17} atoms cm^{-3} for carbon and oxygen, and 1×10^{17} atoms cm^{-3} for sulfur and phosphorus. Atomic concentrations are accurate to within 20% in the alumina layer (using an Al_2O_3 implant standard) and a factor of two in the PbSe/alumina layer (using a ZnSe implant standard). The depth scale for each layer was quantified by measuring the analysis craters for each of the alumina, PbSe/alumina, and Si layers using a stylus profilometer.

Electrical measurements. All field-effect transistors (FETs) were fabricated on p^{++} (100)-oriented Si substrates coated with a 200 nm thick dry thermal oxide layer (Addison Engineering). Metal source and drain electrodes were patterned onto the substrates by standard photolithography and metal deposition. All data presented in this paper utilized Cr/Au electrodes (5 nm Cr/45 nm Au), but Ti, Ag, and Al electrodes were also tested in unsuccessful attempts to suppress the BSE by modifying the FET substrates. Immediately prior to QD film deposition, substrates were sonicated in detergent and isopropanol, rinsed in isopropanol and water, blown dry, and then O_2 plasma cleaned for 5 minutes (Diener Zepto).

Electrical measurements were performed in the dark using a Keithley 2636B source-measure unit controlled by Labview software. Room-temperature measurements were performed using a homebuilt probe station in the glovebox. Variable-temperature measurements utilized a Janis ST-100 cryostat outfitted with a custom five-probe sample mount and Lakeshore Model 325 temperature controller with a calibrated DT-670 Si diode. The base pressure of the cryostat was 5×10^{-8} Torr at 80 K (Pfeiffer HiCube 80 Eco turbopump). FETs were mounted on a thin sapphire window attached to the copper cold finger probe station of the cryostat. Apiezon N thermal grease was applied to all surfaces to ensure good thermal contact. The accuracy of temperature readings was verified by mounting the Si diode directly on a test substrate and measuring the base temperature (80 K). The linear electron mobility was calculated from transfer curves at $V_G = 50$ V and $V_{SD} = 10$ V using the gradual channel approximation equation for transconductance,

$$\left.\frac{dI_D}{dV_G}\right|_{V_{SD}} = \frac{WC_{ox}V_{SD}}{L}\mu_{lin},$$

where $C_{ox} = 17.5$ nF cm^{-2}, and W and L are the channel width (1000 μm) and length (25 μm), respectively.

SUPPLEMENTARY MATERIAL

See the supplementary material for Figures S1–S26, including characterization of EDT-, formate-, SCN-, oxalate-, trimesate-, and BDT-capped QD FETs, V_G sweep rate dependence for BSE-free devices, electrical data vs temperature and QD size, TEM and other supporting data for the high-mobility devices, substrate modification results, GDMS and SIMS data, results of process modifications,

TEM images of the alumina coatings vs thickness, FET data as a function of alumina thickness, results of MNO_3 and other cation and anion treatments of partially infilled QD films, results for alternative ALD infills, and examples of persistent hole transients in H_2S-dosed and alumina-infilled devices.

ACKNOWLEDGMENTS

J.T. acknowledges support from an NSF Graduate Research Fellowship. J. T. and M.G. were supported by the Center for Advanced Solar Photophysics (CASP), an Energy Frontier Research Center funded by the U.S. Department of Energy (DOE), Office of Science, Office of Basic Energy Sciences (BES). A.A. was supported by the UC Office of the President under the UC Laboratory Fees Research Program Collaborative Research and Training Award No. LFR-17-477148. M.L. was supported by the U.S. Department of Energy, Office of Science, Basic Energy Sciences, under Award No. DE-SC0003904. We thank the UCI School of Physical Sciences Center for Solar Energy. SEM and XRD work were performed at the Laboratory for Electron and X-ray Instrumentation (LEXI) at UC Irvine.

AUTHOR DECLARATIONS

Conflict of Interest

The authors have no conflicts to disclose.

Author Contributions

J.T. synthesized the QDs, fabricated the devices, and performed the electrical measurements. M.G. performed FTIR and XRD measurements. A.A. assisted with device fabrication and testing. M.L. conceived and directed the study and assisted with data interpretation. M.L. wrote the manuscript with input from all authors.

Jason Tolentino: Data curation (equal); Formal analysis (equal); Investigation (equal); Writing – review & editing (supporting). **Markelle Gibbs**: Data curation (equal); Formal analysis (equal); Investigation (equal); Writing – review & editing (supporting). **Alex Abelson**: Formal analysis (equal); Investigation (equal); Writing – review & editing (supporting). **Matt Law**: Conceptualization (lead); Data curation (equal); Formal analysis (equal); Funding acquisition (lead); Investigation (equal); Methodology (lead); Project administration (lead); Resources (lead); Supervision (lead); Validation (lead); Visualization (equal); Writing – original draft (lead); Writing – review & editing (lead).

DATA AVAILABILITY

The data that support the findings of this study are available from the corresponding author upon reasonable request.

REFERENCES

[1]F. Hetsch, N. Zhao, S. V. Kershaw, and A. L. Rogach, Mater. Today **16**, 312 (2013).
[2]C. R. Kagan, Chem. Soc. Rev. **48**, 1626 (2019).
[3]D. V. C. B. Murray and C. B. Murray, Science **310**, 86 (2005).
[4]J. M. Luther, M. Law, Q. Song, M. C. Perkins, A. J. Beard, and A. J. Nozik, ACS Nano **2**, 271 (2008).
[5]M. Law, J. M. Luther, Q. Song, B. K. Hughes, C. L. Perkins, and A. J. Nozik, J. Am. Chem. Soc. **130**, 5974 (2008).
[6]M. H. Zarghami, Y. Liu, M. Gibbs, E. Gebremichael, C. Webster, and M. Law, ACS Nano **4**, 2475 (2010).
[7]M. S. Kang, A. Sahu, D. J. Norris, and C. D. Frisbie, Nano Lett. **11**, 3887 (2011).
[8]Y. Liu, M. Gibbs, J. Puthussery, S. Gaik, R. Ihly, H. W. Hillhouse, and M. Law, Nano Lett. **10**, 1960 (2010).
[9]T. P. Osedach, N. Zhao, T. L. Andrew, P. R. Brown, D. D. Wanger, D. B. Strasfeld, L.-Y. Chang, M. G. Bawendi, and V. Bulović, ACS Nano **6**, 3121 (2012).
[10]Y. Liu, J. Tolentino, M. Gibbs, R. Ihly, C. L. Perkins, Y. Liu, N. Crawford, J. C. Hemminger, and M. Law, Nano Lett. **13**, 1578 (2013).
[11]S. J. Oh, N. E. Berry, J.-H. Choi, E. A. Gaulding, H. Lin, T. Paik, B. T. Diroll, S. Muramoto, C. B. Murray, and C. R. Kagan, Nano Lett. **14**, 1559 (2014).
[12]E. L. Rosen, A. M. Sawvel, D. J. Milliron, and B. A. Helms, Chem. Mater. **26**, 2214 (2014).
[13]Y. Zhang, Q. Chen, A. P. Alivisatos, and M. Salmeron, Nano Lett. **15**, 4657 (2015).
[14]A. G. Shulga, L. Piveteau, S. Z. Bisri, M. V. Kovalenko, and M. A. Loi, Adv. Electron. Mater. **2**, 1500467 (2016).
[15]G. Zhou, S. Zhou, Q. Zhu, and N. Zhao, Adv. Electron. Mater. **5**, 1900055 (2019).
[16]P. Xia, D. W. Davies, B. B. Patel, M. Qin, Z. Liang, K. R. Graham, Y. Diao, and M. L. Tang, Nanoscale **12**, 11174 (2020).
[17]A. Abelson, C. Qian, Z. Crawford, G. T. Zimanyi, and M. Law, Nano Lett. **22**, 9578 (2022).
[18]O. Voznyy, S. M. Thon, A. H. Ip, and E. H. Sargent, J. Phys. Chem. Lett. **4**, 987 (2013).
[19]A. Sharma, S. G. J. Mathijssen, E. C. P. Smits, M. Kemerink, D. M. de Leeuw, and P. A. Bobbert, Phys. Rev. B **82**, 075322 (2010).
[20]D. S. Chung, J.-S. Lee, J. Huang, A. Nag, S. Ithurria, and D. V. Talapin, Nano Lett. **12**, 1813 (2012).
[21]M. I. Nugraha, R. Häusermann, S. Watanabe, H. Matsui, M. Sytnyk, W. Heiss, J. Takeya, and M. A. Loi, ACS Appl. Mater. Interfaces **9**, 4719 (2017).
[22]Y. Liu, M. Gibbs, C. L. Perkins, M. H. Tolentino, J. Zarghami, Jr., M. Bustamante, and M. Law Nano Lett. **11**, 5349 (2011).
[23]*CRC Handbook of Chemistry and Physics*, 103rd ed., edited by J. Rumble (CRC Press, Boca Raton, FL, 2022).
[24]H. Sinozaki, R. Hara, and S. Mitsukuri, Bull. Chem. Soc. Jpn. **1**, 59 (1926).
[25]V. Soonsin, A. A. Zardini, C. Marcolli, A. Zuend, and U. K. Krieger, Atmos. Chem. Phys. **10**, 11753 (2010).
[26]V. Hoffmann, M. Kasik, P. K. Robinson, and C. Venzago, Anal. Bioanal. Chem. **381**, 173 (2005).
[27]J. E. R. J. Hinde and R. J. Hinde, Can. J. Chem. **83**, 2005 (2005).
[28]J. H. Song, X. D. Mai, S. Jeong, and Y.-H. Kim, J. Phys. Chem. Lett. **8**, 5259 (2017).